ELSEVIER

Mechanics of Materials 34 (2002) 161–177

MECHANICS OF MATERIALS

www.elsevier.com/locate/mechmat

A constitutive model for the mechanical behavior of a 3D C/C composite

Jérôme Pailhes [1], Gérald Camus *, Jacques Lamon

Laboratoire des Composites Thermostructuraux, UMR 5801 (CNRS-SNECMA-CEA-UB1), 3 Allée de La Boétie, 33600 Pessac, France

Received 30 November 2000; received in revised form 30 September 2001

Abstract

A constitutive model is developed to describe the mechanical behavior of a 3D stitched carbon/carbon composite subjected to complex multiaxial loadings. This model lies within the framework of Continuum Damage Mechanics (CDM) for the description of damage accumulation, and the approach to plasticity for the description of inelastic residual strains induced by the onset of damage. Microstructural observations of the various damage entities provide qualitative data allowing us to formulate physically based simplifying hypotheses. The evolution laws of scalar internal damage variables derived from the components of the compliance tensor are established within a classical thermodynamic framework, using coupled multicriteria expressed in the space of the associated thermodynamic forces. The various processes involved in the non-linear behavior observed under compressive loadings are introduced through the definition of an effective compliance tensor increment. Major advantages and drawbacks of the proposed approach as observed from various validation tests are discussed.

Keywords: 3D carbon/carbon composite; Non-linear behavior; Continuum damage mechanics; Anisotropic damage; Constitutive model

1. Introduction

Carbon fiber-reinforced carbon (C/C) composites represent an important class of high temperature structural materials. They combine a wide range of fibers, matrix materials, reinforcement geometries and processing conditions which results in a large diversity of thermomechanical properties. Nevertheless, a common feature which is always observed among these properties is their non-linear stress–strain response to an applied shear and/or off-axis mechanical loading (Savage, 1993). The development of structural analysis codes aimed at optimizing the design of components made of C/C composites therefore requires to properly incorporate this non-linear behavior. As in the case of ceramic matrix composites, such non-linearities are related to the progressive development of various energy dissipating phenomena collectively termed as damage, i.e. matrix microcracking, fiber/matrix debonding and sliding.

* Corresponding author. Tel.: +33-5-56-84-47-00; fax: +33-5-56-84-12-25.

E-mail address: camus@lcts.u-bordeaux.fr (G. Camus).

[1] Present address: ENSAM-Centre de Bordeaux, Esplanade des Arts et Métiers, 33405 Talence Cedex, France.

0167-6636/02/$ - see front matter
PII: S0167-6636(01)00101-6

Consequently, if some attempts have been made with purely phenomenological approaches (Nguyen et al., 1993; Genin and Hutchinson, 1997), the most reliable constitutive models for the mechanical behavior of C/C materials, as far as complex multiaxial loadings are concerned, have been established within the Continuum Damage Mechanics (CDM) framework (Dumont et al., 1987; Cluzel et al., 1992; Siron et al., 1999). CDM attempts to measure the effects of the internal morphological changes taking place in a material on its mechanical response, through the introduction of an internal state variable, referred to as the damage variable, in the sense of irreversible thermodynamics. Since the early works of Kachanov (1958), CDM approaches based on damage variables derived from the change of the elastic characteristics have been applied to a wide variety of materials such as metals, concrete and fiber-reinforced composites (Krajcinovic, 1989; Lemaître, 1992; Ladevèze, 1994; Chaboche et al., 1995). The C/C composite considered in the present study has a complex fibrous architecture and, besides, exhibits a complex anisotropic damage pattern (Siron and Lamon, 1998), which largely justifies the use of a CDM approach to model its constitutive behavior. The proposed constitutive model complements the work of Siron et al. (1999) by including compressive loadings for which the material also displays significant non-linearities. However, the damage variable introduced in the present model relies on a different definition, in which the state of damage of the material is directly described by the change of the compliance tensor induced by any given loading. Such a definition, first introduced by Ortiz in the case of concrete (Ortiz, 1985), allows to establish the damage kinetics, i.e. the damage evolution laws as a function of the imposed loading, under the form of an explicit scheme, which makes the incorporation of the model easier into appropriate finite-element codes. Microstructural observations of the onset and growth of the damage entities were yet systematically performed in conjunction with this macroscopic approach, in order to provide guidelines for the formulation of physically based simplifying hypotheses from which the constitutive equations were then derived. Physical consistency was thus added to the thermodynamic consistency brought by the thermodynamic framework used to establish the CDM-based constitutive model.

2. Material and experimental results

The 3D C/C composite was processed by Snecma-moteurs (Le Haillan, France) by chemical vapor infiltration of a pyrocarbon matrix into a fibrous preform consisting of a stack of ex-PAN carbon-fiber woven fabrics (8-H satin) stitched in the perpendicular direction. In what follows and throughout the text, subscripts 1 and 2 will refer to the warp and the weft direction, respectively (Fig. 1). The mechanical behavior within the plane of the plies (i.e. plane $(1,2)$) was evaluated by means of tests performed at various loading angles from the fiber axes, in tension, compression and cyclic tension/compression. Specimen design, test procedure and strain measurement methods have been thoroughly described in previous studies (Siron, 1996; Siron et al., 1999). It is yet worth mentioning that all the tests were performed at a constant low displacement rate of $0.05\ \text{mm}\ \text{min}^{-1}$, ensuring quasi-static loading conditions.

The as-processed composite displays, in addition to a residual porosity inherent to the CVI process, two distinct families of thermally induced microcracks (Fig. 2): (i) intra-bundle cracks located near the fiber-matrix interface and (ii) inter-bundle cracks located between perpendicular tows. The stress–strain behavior of the material tested in uniaxial tension at various angles to the fiber directions appears to be essentially non-linear and strongly anisotropic (Figs. 3 and 4). The curves

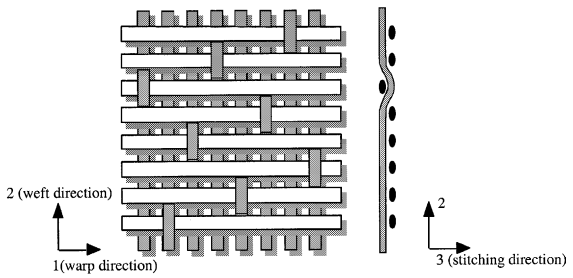

Fig. 1. 8-H satin weave pattern and related coordinate system.

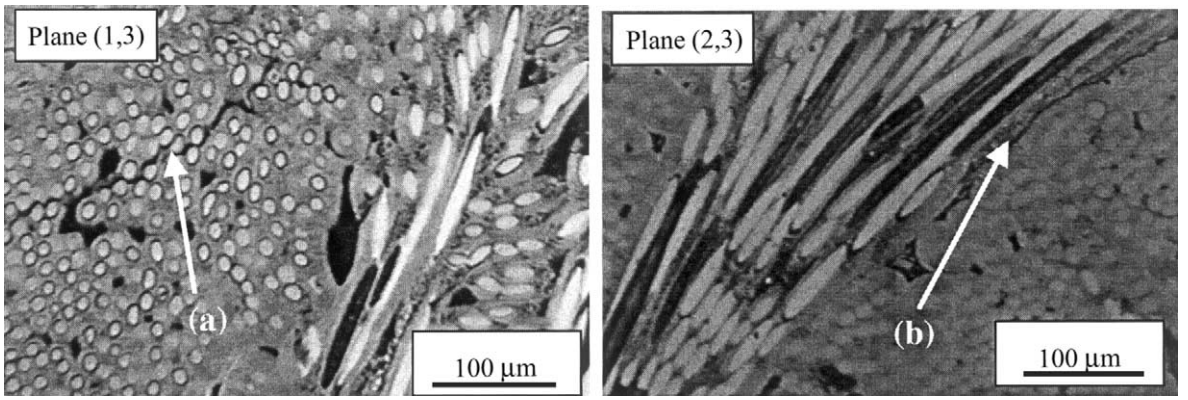

Fig. 2. Optical micrographs of the as-received 3D C/C composite showing thermally induced preexisting microcracks: (a) infra-bundle cracks; (b) inter-bundle cracks.

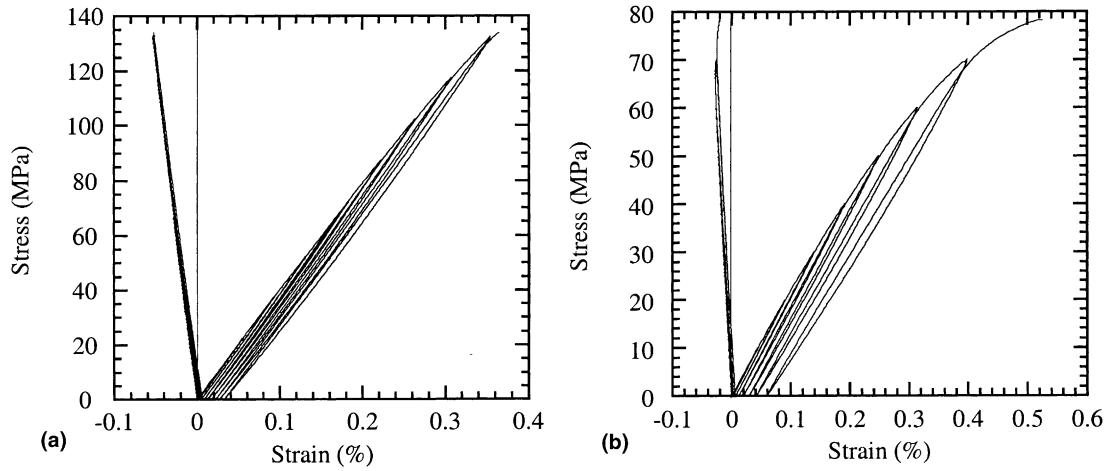

Fig. 3. Mechanical behavior of the 3D C/C in on-axis tension with interposed loading/unloading cycles: (a) applied load parallel to direction 1 (warp direction); (b) applied load parallel to direction 2 (weft direction).

displayed in Fig. 3 also reveal different behavior in the two fiber directions, most likely related to the stitching process of the fibrous preform which induces more undulated bundles along the weft direction (direction 2). The dependence of the applied stress as a function of the in-plane transverse strain observed in Fig. 3 shows that the off-diagonal component of the compliance tensor, S_{12}, may be considered, with a good approximation, as remaining constant. Thus, damage-induced deviation in the Poisson's ratio appears to only depend on the longitudinal behavior. This feature, which is commonly observed in the case of fiber reinforced composites with compliant matrices, e.g. carbon or polymer, is likely related to the fact that the transverse behavior is dominated by the Poisson's contraction of the fiber bundles. Unloading/reloading cycles performed during the tests evidence a progressive decrease of the material's moduli related to the evolution of damage, as well as significant residual strains upon unloading. Given the small width of the hysteresis loops observed upon cycling, these residual strains may be mainly attributed to the interaction of two phenomena: (i) the release of thermal residual stresses present from processing and (ii) a partial re-

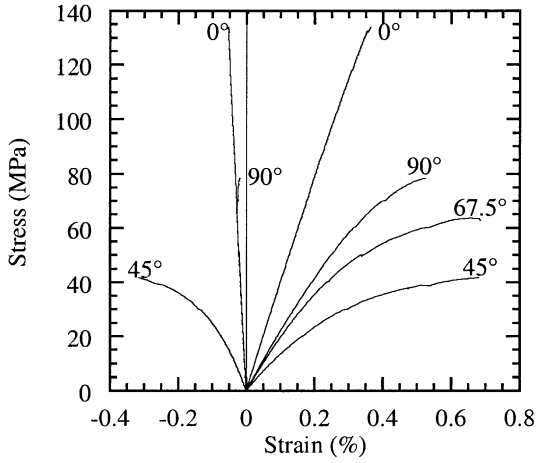

Fig. 4. Mechanical behavior of the 3D C/C in off-axis monotonic tension for various loading angles from direction 1.

alignment of the fiber bundles (Siron and Lamon, 1998).

Typical microstructural changes taking place in the material when tested in tension under various loading angles as well as in shear are schematically summarized in Fig. 5. The two modes of intra-bundle and inter-bundle cracks already present from processing, referred to as a-cracks and b-cracks in Fig. 5, were found to multiply during the tests, following this chronological order, whereas a third mode appeared to take place at higher stresses. This last family of cracks, referred to as c-cracks in Fig. 5, may be viewed as a coalescence of

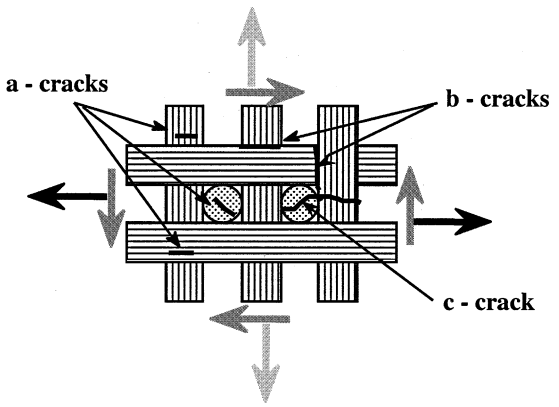

Fig. 5. Schematic diagram summarizing the three families of cracks observed during tensile and shear tests.

two adjacent intra-bundle cracks. Consequently, these cracks of the third mode were on the average the longest, i.e. about 1 mm in mean length. Finally, it should be emphasized that the orientation of these three families of load-induced microcracks appeared to be mainly imposed by the direction of the bundles rather than by the direction of the applied load.

As illustrated by Fig. 6, the compressive behavior is non-linear whatever the loading angle, i.e. even when the load is applied along the fiber axes. In this latter case, a closer examination of the stress–strain response allowed us to attribute this overall non-linearity to a combination of damage, as attested by acoustic emission monitoring, and non-linear elasticity likely related to a reversible microbuckling of the fiber bundles, as commonly observed in carbon/epoxy composites (Allix et al., 1994). Similarly to tests performed in tension, residual strains are also observed upon unloading. Regarding the damage modes taking place in compression, microstructural observations essentially revealed an important development of intra-bundle cracks.

As graphically depicted in Fig. 7, reverse tension/compression tests evidence a stiffening of the material's response at the beginning of the compression domain. In each of the tests performed, however, the initial modulus was never fully recovered, which suggests that this stiffening phase is linked to an only partial closure of the microcracks generated in tension. Furthermore, the prolongation of the unloading sequences in the compression domain appears to modify the subsequent tensile behavior, i.e. when comparisons are made with similar monotonic tensile tests. This last feature tends to indicate a noticeable coupling between the two damage modes.

3. Description of the model

3.1. General hypotheses and damage variables

The model is established under the usual restrictive assumption of small isothermal displacements and quasi-static loadings (i.e. the damage phenomena are assumed to be time-independent)

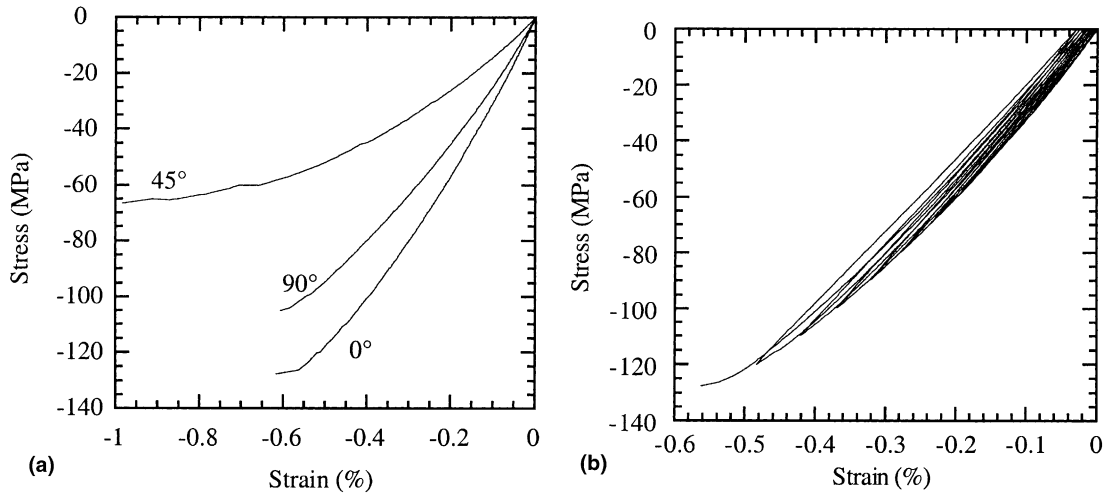

Fig. 6. Mechanical behavior of the 3D C/C in compression: (a) monotonic at various loading angles from direction 1; (b) cycled with the load applied parallel to direction 1.

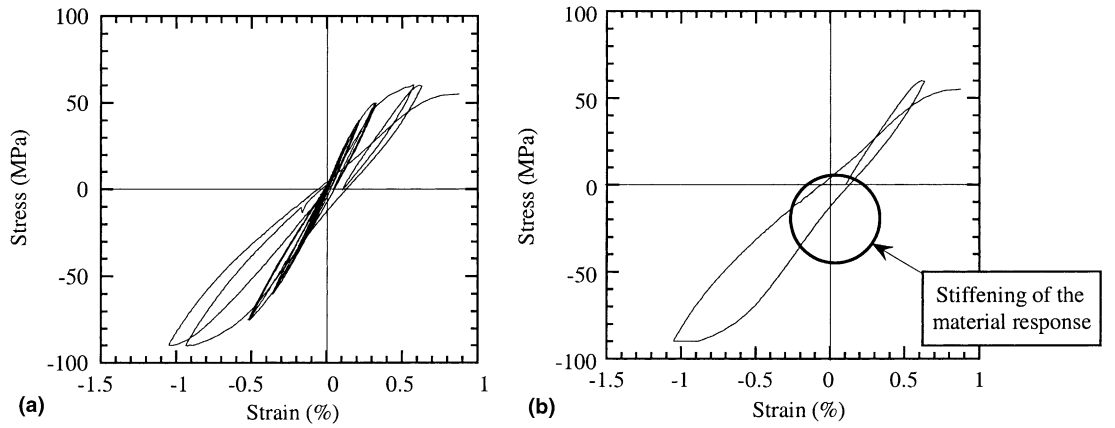

Fig. 7. (a) Off-axis cyclic tension/compression test performed at 67.5° from direction 1; (b) characterization cycle taken out from the test.

for an average plane-stress state within the plane of the plies. Likewise, the only non-linear dissipative mechanisms considered are those attributed to the damage phenomena. Frictional sliding, responsible for the hysteretic effects observed from interposed loading/unloading cycles, is therefore neglected, i.e. linear elasticity is assumed to hold if the damage state does not change.

The strain tensor $\boldsymbol{\varepsilon}$ is classically split into elastic reversible strains and "inelastic" residual strains, according to:

$$\boldsymbol{\varepsilon} = \boldsymbol{\varepsilon}^{e} + \boldsymbol{\varepsilon}^{p}. \tag{1}$$

In what follows, $\boldsymbol{\sigma}$ will denote the stress tensor whereas the Voigt contracted notation (with $\varepsilon_6 = 2\varepsilon_{12}$) will be used throughout the text.

Following Ortiz (1985), we choose to define the state of damage of the material by the change of the compliance tensor induced by the imposed loading. The compliance tensor may then be decomposed as follows:

$$\mathbf{S} = \mathbf{S}^{0} + \Delta\mathbf{S}, \tag{2}$$

where $\mathbf{S}^0$ stands for the initial compliance tensor of the as-received material and $\Delta\mathbf{S}$ represents the added compliance due to damage. This fourth rank symmetrical tensor is thus defined as the internal variable representing the current state of damage in the material (Baste and Audoin, 1991).

On the basis of the experimental results described in the preceding section, it may then be further assumed that:

(i) the fiber directions naturally represent the local orthotropy axes of the composite and this orthotropic symmetry is maintained throughout the damage processes;
(ii) the off-diagonal component of the compliance tensor, S_{12} remains constant throughout the tests.

Given these hypotheses, the constitutive law of the material may be simply formulated with respect to the material principal coordinate system (Fig. 1). Consequently, most of the equations developed hereafter are not general tensorial expressions. Likewise, the diagonal components of the internal damage variable $\Delta\mathbf{S}$ may be used to define scalar variables. By normalizing these components by their respective initial values, in order to deal with non-dimensional variables, the three following scalar damage variables are thus considered:

$$\omega_i = \frac{\Delta S_{ii}}{S^0_{ii}}, \quad i = 1, 2, 6. \tag{3}$$

3.2. Compressive behavior

The incorporation of compressive loadings in the constitutive law obviously requires taking into account the three main phenomena identified during the compression tests: (i) non-linear elasticity, (ii) a partial deactivation of the damage present from processing and/or produced in tension and (iii) the onset of damage accompanied by residual strains occurring at the macroscale once the partial crack closure has been completed.

Following a suggestion initially made by Allix et al. (1994), it appears that the experimental compliance change related to the non-linear elastic behavior may be simply expressed in the following manner:

$$S_{ii} \to S^0_{ii}(1 + \gamma_i\langle -\sigma_i\rangle), \quad i = 1, 2, \text{ no summation.} \tag{4}$$

The symbol $\langle\cdot\rangle$ signifies the McAuley bracket with its usual definition: $\langle x\rangle = (1/2)(x + |x|)$, $\gamma_i (i = 1, 2)$ are two constants governing the reversible increase of the compressive compliance.

An active/passive unilateral damage condition is next considered, through the introduction of an effective compliance tensor, $\Delta\hat{\mathbf{S}}$, defined as follows (Chaboche et al., 1995):

$$\Delta\hat{\mathbf{S}} = \mathbf{Q} : \Delta\mathbf{S}, \tag{5a}$$

where $\mathbf{Q}$ represents a fourth rank diagonal tensor:

$$\mathbf{Q} = \mathrm{diag}[Q(\hat{\sigma}_1), Q(\hat{\sigma}_2), Q(\hat{\sigma}_6)] \tag{5b}$$

and Q defines the following step function:

$$\begin{aligned} Q(x) &= 1 \quad \text{if } x \geqslant 0, \\ Q(x) &= \eta \quad \text{if } x < 0 \end{aligned} \tag{5c}$$

with η $(0 \leqslant \eta \leqslant 1)$ being a coefficient accounting for the amount of damage deactivated, whereas $\hat{\sigma}_i$ $(i = 1, 2, 6)$ stands for equivalent deactivation stresses.

On the basis of the experimental results previously described, we may assume that both crack closure and damage evolution occur at a similar stress threshold related to the thermal residual stresses present from processing. In order to deal with this basic assumption, a second-order tensor of constant terms (i.e. the threshold stresses), $\boldsymbol{\sigma}^{\mathrm{r}}$, is introduced. In a first approximation, an active/passive condition based on a normal stress criterion may be retained in the case of tensile and compressive loadings performed along the fiber axes (Chaboche et al., 1995). Experimental observations have shown that load-induced microcracks are mostly orientated parallel and/or perpendicular to the orthotropy axes whatever the imposed loading, i.e. even when a shear component is present. If the shear stresses are reversed, the principal stresses just interchange their directions, i.e. at $\pm 45°$ from the orthotropy axes, which reasonably leads one to state that damage still remains active. This justifies the approximation that the influence of damage due to shearing on the effective shear compliance is the same after load reversal. A zero

value is therefore assigned to the threshold stress σ_6^r, hence:

$$\begin{aligned} &\hat{\sigma}_i = \sigma_i - \sigma_i^r, \quad i = 1,2, \\ &\hat{\sigma}_6 = \sigma_6^r = 0. \end{aligned} \tag{6}$$

By combining Eqs. (3), (4), (5a)–(5c), the complete expression defining the components of the effective compliance tensor increment finally reduces to:

$$\begin{cases} \Delta\hat{S}_{ii} = S_{ii}^0 Q((\hat{\sigma}_i)\omega_i + \gamma_i\langle -\sigma_i\rangle), \\ \Delta\hat{S}_{66} = S_{66}^0\omega_6, \\ \Delta\hat{S}_{12} = 0, \end{cases}$$
$$i = 1,2, \text{ no summation.} \tag{7}$$

3.3. Damage kinetics and constitutive law

A classical way to formulate the constitutive equations describing the damage kinetics, i.e. the increase laws of the damage variables as a function of the imposed loading, is to consider the framework of the thermodynamics of irreversible processes, in which two potentials are introduced (Bataille and Kestin, 1979; Germain et al., 1983):

- the thermodynamic potential, written as a function of the state variables, which defines the state laws and the conjugate variables associated with the state variables;
- the dissipation potential, written in the space of the associated variables, which accounts for the kinetic laws of evolution of the dissipative internal state variables.

3.3.1. Thermodynamic potential and constitutive law

The present definition of damage based on the change of the compliance tensor naturally dictates the choice of $\boldsymbol{\sigma}$ and T, respectively the stress tensor and the absolute temperature, as the "observable" state variables and thus of a thermodynamic potential based on the Gibbs free energy. Referring to the strain partition assumption previously made (Eq. (1)), this thermodynamic potential Ψ is in turn written as the sum of two terms, Ψ_e and Ψ_p, respectively, linked to the elastic behavior and to the inelastic residual strains:

$$\Psi = \Psi_e(\boldsymbol{\sigma}, \Delta\mathbf{S}) + \Psi_p(p), \tag{8}$$

where p is a scalar variable representing the accumulated residual strain. The kinetic equations describing the rate of change of the residual strains are described in a later section. The assumed existence of a non-linear elastic component in the compressive behavior also leads to the introduction of the following partition of Ψ_e:

$$\Psi_e(\boldsymbol{\sigma}, \Delta\mathbf{S}) = \Psi_e^*(\boldsymbol{\sigma}, \Delta\mathbf{S}) + \alpha(\langle -\sigma_1\rangle, \langle -\sigma_2\rangle), \tag{9}$$

where α represents a positive-valued scalar function such that:

$$\frac{\partial^2\alpha}{\partial\sigma_i^2} = 2S_{ii}^0\gamma_i\langle -\sigma_i\rangle, \quad i = 1,2. \tag{10}$$

According to standard arguments, conjugate variables associated with the state variables are derived from the thermodynamic potential:

$$\boldsymbol{\varepsilon}^e = \left(\frac{\partial\Psi}{\partial\boldsymbol{\sigma}}\right)_{\omega_i} = \left(\frac{\partial\Psi_e}{\partial\boldsymbol{\sigma}}\right)_{\omega_i}, \tag{11a}$$

$$Y_i = \left(\frac{\partial\Psi}{\partial\omega_i}\right)_{\sigma} = \left(\frac{\partial\Psi_e}{\partial\omega_i}\right)_{\sigma}. \tag{11b}$$

The variables Y_i are the generalized thermodynamic forces conjugate to the damage variables ω_i. Within the CDM framework, these variables have the precise meaning of energy, released per volume, due to the advancement of damage and are thus referred to as "energy density release rates" (Lemaître, 1992).

It is assumed that the component of the thermodynamic potential related to damage, Ψ_e^*, may be expanded as a polynomial function, quadratic in stresses and linear in damage variable, defined as follows (Harris et al., 1989; Talreja, 1991):

$$\begin{aligned} \Psi_e^* = {} & \frac{1}{2}\boldsymbol{\sigma} : (\mathbf{S}^0 + \mathbf{Q} : \Delta\mathbf{S}) : \boldsymbol{\sigma} \\ & + (\boldsymbol{\sigma} - \boldsymbol{\sigma}^r) : (\mathbf{I} - \mathbf{Q}) : \Delta\mathbf{S} : \boldsymbol{\sigma}^r \\ & - \frac{1}{2}\boldsymbol{\sigma}^r : \mathbf{Q} : \Delta\mathbf{S} : \boldsymbol{\sigma}^r + K. \end{aligned} \tag{12}$$

Such a definition represents the most general and simplest form accounting for the observed mechanical behavior, while preserving an adequate physical coherency. Hence, the two linear terms in $\boldsymbol{\sigma}$ and $\Delta\mathbf{S}$ insure strain continuity when deactivation takes place and a coherent definition of the thermodynamic forces associated with compres-

sive damage. K is a constant introduced to allow the thermodynamic potential to be always positive. It may be easily recognized that, in the case of a residual stress free material (i.e. $\boldsymbol{\sigma}^{\mathrm{r}} = 0$), if K is taken to be zero, the usual definition of a thermodynamic potential merged with the complementary strain energy density function is recovered (Fung, 1965).

Eq. (11a) establishes the constitutive law of the material:

$$\boldsymbol{\varepsilon}_{\mathrm{e}} = \left(\frac{\partial \Psi_{\mathrm{e}}}{\partial \boldsymbol{\sigma}}\right)_{\omega_i} = (\mathbf{S}^0 + \mathbf{Q} : \Delta\mathbf{S}) : \boldsymbol{\sigma} + (\mathbf{I} - \mathbf{Q}) : \Delta\mathbf{S} : \boldsymbol{\sigma}^{\mathrm{r}} + \frac{\partial \alpha}{\partial \boldsymbol{\sigma}} \tag{13}$$

or, under an expanded form:

$$\begin{aligned}
\varepsilon_1^{\mathrm{e}} &= S_{11}^0(1 + Q(\hat{\sigma}_1)\omega_1 + \gamma_1\langle -\sigma_1\rangle)\sigma_1 \\
&\quad + S_{11}^0(1 - Q(\hat{\sigma}_1))\omega_1\sigma_1^{\mathrm{r}} + S_{12}^0\sigma_2, \\
\varepsilon_2^{\mathrm{e}} &= S_{22}^0(1 + Q(\hat{\sigma}_2)\omega_2 + \gamma_2\langle -\sigma_2\rangle)\sigma_2 \\
&\quad + S_{22}^0(1 - Q(\hat{\sigma}_2))\omega_2\sigma_2^{\mathrm{r}} + S_{12}^0\sigma_1, \\
\varepsilon_6^{\mathrm{e}} &= S_{66}^0(1 + \omega_6)\sigma_6.
\end{aligned} \tag{14}$$

The thermodynamic forces Y_i represent the driving forces accounting for the kinetic laws of evolution of the dissipative damage variables. In order to derive from Eq. (11b) a physically and thermodynamically coherent expression for the variables Y_i (i.e. $Y_i \geqslant 0$, $Y_i = 0$ when damage does not propagate), it is then necessary to split the thermodynamic potential into three parts: a "tension potential" Ψ_{t}, a "compression" potential Ψ_{c} and a potential identical for both tension and compression behaviors Ψ_{tc} (Ladevèze et al., 1994). Introducing the classical decomposition of Eq. (12) in the following manner:

$$\begin{aligned}
&\sigma_i^2 = \langle\sigma_i\rangle^2 + \langle -\sigma_i\rangle^2, \\
&\sigma_i - \sigma_i^{\mathrm{r}} = \langle\sigma_i - \sigma_i^{\mathrm{r}}\rangle - \langle\sigma_i^{\mathrm{r}} - \sigma_i\rangle, \quad i = 1, 2,
\end{aligned} \tag{15}$$

yields, with a little algebra:

$$\Psi_{\mathrm{t}} = \frac{1}{2}\left(\langle\sigma_1\rangle^2 S_{11}^0(1 + \omega_1) + \langle\sigma_2\rangle^2 S_{22}^0(1 + \omega_2)\right),$$

$$\Psi_{\mathrm{c}} = \frac{1}{2}\sum_{i=1}^{2}\left(\langle -\sigma_i\rangle^2 - \sigma_i^{r^2}\right)S_{ii}^0 Q(\hat{\sigma}_i)\omega_i - 2\langle\sigma_i^{\mathrm{r}} - \sigma_i\rangle\sigma_i^{\mathrm{r}} S_{ii}^0(1 - Q(\hat{\sigma}_i))\omega_i + \langle -\sigma_i\rangle^2 S_{ii}^0, \tag{16}$$

$$\Psi_{\mathrm{tc}} = S_{12}^0\sigma_1\sigma_2 + \sigma_6^2 S_{66}^0(1 + \omega_6).$$

By introducing the notation Y_i^+ and Y_i^- $(i = 1, 2)$ to define tensile and compressive thermodynamic forces, respectively, and making use of Eqs. (11b) and (16) one finally obtains:

$$Y_1^+ = \left(\frac{\partial \Psi_{\mathrm{t}}}{\partial \omega_1}\right)_{\sigma} = \frac{1}{2}S_{11}^0\langle\sigma_1\rangle^2, \tag{17}$$

$$\begin{aligned}
Y_1^- &= \left\langle \frac{\partial \Psi_{\mathrm{c}}}{\partial \omega_1}\right\rangle_{\sigma} \\
&= \frac{1}{2}S_{11}^0\Big\langle Q(\hat{\sigma}_1)\left(\langle -\sigma_1\rangle^2 - \sigma_1^{r^2}\right) \\
&\quad - 2(1 - Q(\hat{\sigma}_1))\langle\sigma_1^{\mathrm{r}} - \sigma_1\rangle\sigma_1^{\mathrm{r}}\Big\rangle,
\end{aligned}$$

$$Y_2^+ = \left(\frac{\partial \Psi_{\mathrm{t}}}{\partial \omega_2}\right)_{\sigma} = \frac{1}{2}S_{22}^0\langle\sigma_2\rangle^2,$$

$$\begin{aligned}
Y_2^- &= \left\langle \frac{\partial \Psi_{\mathrm{c}}}{\partial \omega_2}\right\rangle_{\sigma} \\
&= \frac{1}{2}S_{22}^0\Big\langle Q(\hat{\sigma}_2)\left(\langle -\sigma_2\rangle^2 - \sigma_2^{r^2}\right) \\
&\quad - 2(1 - Q(\hat{\sigma}_2))\langle\sigma_2^{\mathrm{r}} - \sigma_2\rangle\sigma_2^{\mathrm{r}}\Big\rangle,
\end{aligned}$$

$$Y_6 = \left(\frac{\partial \Psi_{\mathrm{tc}}}{\partial \omega_6}\right)_{\sigma} = \frac{1}{2}S_{66}^0\sigma_6^2.$$

It may be easily checked that the thermodynamic forces Y_1^- and Y_2^- thus defined have a zero value as long as the partial deactivation stresses σ_i^{r} $(i = 1, 2)$ have not been reached.

3.3.2. Dissipation potential and damage kinetics

In order to be thermodynamically consistent, the Clausius–Duhem's inequality, which contains both the first and the second law of thermodynamics and accounts for positive dissipation, has to be verified. In the present case of damage being considered as the only dissipative phenomenon and for an isothermal process, it may be shown that this law is automatically checked if (and only if) the complementary laws describing the damage kinetics obey the conditions $\dot{\omega}_i \geqslant 0$ $(i = 1, 2, 6)$. This requirement of positive internal dissipation gives motivation to postulate the existence of a dissipation potential, written in the generalized

space of the associated thermodynamic forces, from which the damage kinetic laws are derived. Within the simplifying assumption presently made of a time independent process, an associated framework may be used, in which the dissipation potential is replaced by damage criterion functions describing the surface limiting the undamaged domain (Ladevèze, 1994; Chaboche et al., 1995). In addition, the choice of coupled multiple criteria, one for each damage variable, has also been retained:

$$\begin{aligned}\omega_1 &= f_1(\underline{Y_1^*}),\\ \omega_2 &= f_2(\underline{Y_2^*}),\\ \omega_6 &= f_1(\underline{Y_6^*})\end{aligned} \tag{18a}$$

with the notation

$$\underline{x(t)} = \mathrm{Sup}_{\tau \leqslant t}(x(\tau)), \tag{18b}$$

where f_1, f_2, and f_6 represent the principal damage threshold functions, whereas Y_i^* $(i = 1, 2, 6)$ are scalar functions of the thermodynamic forces Y_i $(i = 1, 2, 6)$ representing the equations of the damage surfaces. The supremum taken over the Y_i^* is aimed at storing the loading history by stating that the values at a given time t of the damage variables will increase only if the maximum value of Y_i^* reached during previous loadings is exceeded. Positive dissipation together with the assumption that the damage kinetic laws are derived from a multisurface potential require the scalar functions f_i $(i = 1, 2, 6)$ to be positive and monotonically increasing and the damage surface to be positive and at least star-convex with respect to the origin (Matzenmiller et al., 1995).

The following approximation of the equations describing the damage surfaces is then considered:

$$\begin{aligned}Y_1^* &= Y_1 + g_{12}(\underline{Y_2})Y_2 + g_{16}(\underline{Y_6})Y_6,\\ Y_2^* &= Y_2 + g_{21}(\underline{Y_1})Y_1 + g_{26}(\underline{Y_2})Y_6,\\ Y_6^* &= Y_6 + g_{61}(\underline{Y_1})Y_1 + g_{62}(\underline{Y_2})Y_2\end{aligned} \tag{19a}$$

with

$$Y_i = Y_i^+ + Y_i^-, \quad i = 1, 2, \tag{19b}$$

where g_{ij} are non-dimensional positive scalar functions accommodating the coupling of growth for the individual damage variables in the various damage modes. Following a formalism initially introduced for a 2D SiC/SiC composite (Camus, 2000), these coupling terms have not been a priori described by constant coefficients as usually suggested in many cases, for the microstructural observations revealed damage entities of different characteristic sizes and surrounding media taking place sequentially under a given applied load. Each of these damage entities should thus be expected to influence differently the variation of the compliance tensor components. Eq. (19b) establishes the couplings between the damage kinetics in tension and compression which, in the absence of a sound experimental guidance, have been chosen under the simplest possible, yet realistic, form.

3.4. Residual strains

As pointed out in the experimental section, the "inelastic" residual strains observed upon unloading result from phenomena which have nothing in common with the classical plasticity of metallic materials. Nevertheless, it is possible to describe these damage-induced residual strains through the use of a formalism derived from the general plasticity theory (Lemaître and Chaboche, 1985; Lubliner, 1990). Such an approach, more phenomenological than the previous one, then justifies to choose a priori a simple formulation "associated standard with isotropic hardening", which has already been successfully applied to different composite materials (Cluzel et al., 1992; Allix et al., 1994; Siron et al., 1999).

Within this framework, the "plastic" potential Ψ_p only depends on the scalar variable p which represents the accumulated residual strains and whose conjugate variable is the isotropic hardening variable R. The "plastic" dissipation potential is merged with a criterion threshold function, h, defined by:

$$h = \sigma_{eq} - R(p) - R_0, \tag{20}$$

where R_0 represents the initial size of the elastic domain, σ_{eq} defines the equation of the threshold surface limiting this domain, whereas $R(p)$ denotes the hardening function.

In order to take into account the different behaviors in tension and in compression, σ_{eq} is

developed under the general form of a second degree polynomial function:

$$\sigma_{\mathrm{eq}} = (\boldsymbol{\sigma} : \mathbf{M} : \boldsymbol{\sigma})^{1/2} + \mathbf{N} : \boldsymbol{\sigma}, \tag{21}$$

in which $\mathbf{M}$ and $\mathbf{N}$ stand for fourth- and second-order tensors, respectively. Given the orthotropic symmetry of the material on the one hand, and the absence of transverse inelastic strains in tension on the other hand, these two tensors are taken to be diagonal. Besides, as it may be reasonably assumed that the residual shear strains are independent of the sign of the imposed shear loading, the linear term in σ_6 is taken to be zero.

These considerations finally reduce the above equation to:

$$\sigma_{\mathrm{eq}} = \sqrt{\sigma_1^2 + a^2\sigma_2^2 + b^2\sigma_6^2} + c\sigma_1 + d\sigma_2, \tag{22}$$

where parameters a, b, c, d are non-dimensional constants characteristic of the material.

The normality rule of the standard framework prescribes the existence of a plastic multiplier λ such that:

$$\dot{\boldsymbol{\varepsilon}}^{\mathrm{p}} = \dot{\lambda}\frac{\partial h}{\partial \boldsymbol{\sigma}}, \tag{23a}$$

$$\dot{p} = -\dot{\lambda}\frac{\partial h}{\partial R} = \dot{\lambda}. \tag{23b}$$

Plastic flow (i.e. $\dot{p} > 0$) takes place under the conditions $h = 0$ and $\dot{h} = 0$, which yields:

$$\dot{p} = \dot{\lambda} = H(h)\frac{\langle \dot{\sigma}_{\mathrm{eq}} \rangle}{R'(p)}, \tag{24}$$

where H represents the Heaviside function:

$$H(x) = 0 \quad \text{if } x < 0,$$
$$H(x) = 1 \quad \text{if } x \geqslant 0$$

by combining Eqs. (23a) and (24), one finally obtains:

$$\dot{\sigma}_{\mathrm{eq}} = \frac{\sigma_1\dot{\sigma}_1 + a^2\sigma_2\dot{\sigma}_2 + b^2\sigma_6\dot{\sigma}_6}{\sqrt{\sigma_1^2 + a^2\sigma_2^2 + b^2\sigma_6^2}} + c\dot{\sigma}_1 + d\dot{\sigma}_2 \tag{25a}$$

and

$$\dot{\varepsilon}_1^{\mathrm{p}} = H(h)\frac{\langle \dot{\sigma}_{\mathrm{eq}} \rangle}{R'(p)}\left(\frac{\sigma_1}{\sqrt{\sigma_1^2 + a^2\sigma_2^2 + b^2\sigma_6^2}} + c\right),$$

$$\dot{\varepsilon}_2^{p} = H(h)\frac{\langle \dot{\sigma}_{\mathrm{eq}} \rangle}{R'(p)}\left(\frac{a^2\sigma_2}{\sqrt{\sigma_1^2 + a^2\sigma_2^2 + b^2\sigma_6^2}} + d\right),$$

$$\dot{\varepsilon}_6^{p} = H(h)\frac{\langle \dot{\sigma}_{\mathrm{eq}} \rangle}{R'(p)}\left(\frac{b^2\sigma_6}{\sqrt{\sigma_1^2 + a^2\sigma_2^2 + b^2\sigma_6^2}}\right). \tag{25b}$$

3.5. Failure criterion

The description of a true rupture theory transposable at the level of real structures is beyond the scope of this paper. The present purpose is therefore restricted to the description of the ultimate damage state of specimens subjected to uniform stress fields before the critical conditions, i.e. slightly before the onset of a macrocrack leading to final rupture. Ultimate failure of the C/C composite may be attributed to different local mechanisms such as fiber ruptures, damage saturation, delamination and macrobucking. A multicriterion depending on the type of loading and relating the different rupture criteria to different rupture mechanisms has thus been adopted.

3.5.1. Tensile loading

Under pure tension, final failure of the composite apparently results from a brittle fracture of the fiber bundles and may therefore be related to a critical stress. In order to take into account the so called "composite effect", i.e. a damage-induced progressive stress redistribution to the fibers, it seems appropriate to express this critical stress in terms of an effective stress. The effective stress tensor, $\tilde{\boldsymbol{\sigma}}$, is related to the damage variables in the classical sense of CDM through a simple relationship (Lemaître, 1992; Ladevèze, 1994):

$$\mathbf{S}^0 : \tilde{\boldsymbol{\sigma}} = \mathbf{S} : \boldsymbol{\sigma} \quad \Rightarrow \quad \tilde{\boldsymbol{\sigma}} = \mathbf{S}^{0^{-1}} : \mathbf{S} : \boldsymbol{\sigma}, \tag{26}$$

which yields, in the case of tensile loadings and after some simplifications:

$$\tilde{\sigma}_i \cong (1 + \omega_i)\sigma_i, \quad i = 1, 2. \tag{27}$$

Fracture is assumed to take place when a critical value $\tilde{\sigma}_i^{\mathrm{f}}$ is reached: $\tilde{\sigma}_i = \tilde{\sigma}_i^{\mathrm{f}}$ $(i = 1, 2)$.

3.5.2. Shear loadings

As it may be observed from the stress/strain curves obtained from a Iosipescu shear test (Siron and Lamon, 1998) and/or from 45° off-axis tests, rupture roughly follows a more or less pronounced plateau like behavior. This behavior corresponds to an instability stage (i.e. $\dot{\sigma}_6 = 0$ with $\dot{\varepsilon}_6 \neq 0$) during which damage increases up to a critical saturation value (Ladevèze et al., 1994). This is in line with the fact that, under pure shear, the matrix is stressed more than the fibers. Consequently, the influence of a shear component on the rupture behavior may be introduced through a critical shear damage value, ω_6^{f}, obtained at the instability peak point.

3.5.3. Compressive loadings

Results obtained from the compression tests suggest that each compressive component plays a part in the rupture behavior. Following a suggestion made in (Ladevèze et al., 1994), a rupture criterion based on a maximum value of the compression energy is therefore retained This compression energy, W_{c} is directly derived from the expression of the thermodynamic potential and may be expressed as follows:

$$W_{\mathrm{c}} = -\frac{1}{2}\left(\langle -\sigma_1\rangle\varepsilon_1^{\mathrm{e}} + \langle -\sigma_2\rangle\varepsilon_2^{\mathrm{e}}\right). \tag{28}$$

Rupture is supposed to occur when W_{c} reaches a critical value, denoted $W_{\mathrm{c}}^{\mathrm{f}}$, which may be determined experimentally by a simple on-axis compression test.

3.5.4. Global rupture criterion

Finally, under complex multiaxial loadings, it is assumed that rupture occurs as soon as one of the failure criteria described above is reached, hence:

$$\begin{aligned} r_i &= \frac{\tilde{\sigma}_i}{\tilde{\sigma}_i^{\mathrm{f}}} - 1, \quad i = 1,2, \\ r_6 &= \frac{\omega_6}{\omega_6^{\mathrm{f}}} - 1, \\ r_0 &= \frac{W_{\mathrm{c}}}{W_{\mathrm{c}}^{\mathrm{f}}} - 1, \end{aligned} \tag{29a}$$

$$F = \mathrm{Sup}_i(r_i)\begin{cases} \geqslant 0 & \text{failed} \\ < 0 & \text{unfailed.} \end{cases} \tag{29b}$$

4. Application to the 3D C/C material

4.1. Identification of the model

The identification of the functions and parameters describing the model is performed with the help of the experimental results displayed in Section 2.

The first step is to assess the initial compliance coefficients (S_{11}^0, S_{22}^0, S_{66}^0 and S_{12}^0) and the principal damage threshold functions (f_1, f_2 and f_6). This is done by considering the stress–strain response of the two on-axis tensile tests and of the 45° off-axis compression test, and by plotting the change of the damage variables ω_i $(i = 1,2,6)$ (derived from the loading/unloading cycles), as a function of their respective thermodynamic forces Y_i $(i = 1,2,6)$ (Fig. 8). The assessment of the shear damage function f_6 from a 45° off-axis compression test follows from the statement that, in the course of this test, the stresses σ_1 and σ_2 appear to be always lower, in absolute value, than their respective threshold σ_1^{r} and σ_2^{r} (whose identification is described thereafter). Application of Eq. (17) thus implies that Y_1 and Y_2 always remain equal to zero. Appropriate forms of evolution law fitting the data shown in Fig. 8 have been established as:

$$\omega_i = f_i(Y_i^*) = \left(\frac{Y_i^*}{Y_i^{\mathrm{s}}}\right)^{a_i}, \quad i = 1,2,6, \tag{30}$$

where the coefficients Y_i^{s} and a_i are normalizing forces and shape exponents, respectively.

The assessment of the parameters describing the compressive behavior, $\gamma_i, \sigma_i^{\mathrm{r}}$ $(i = 1,2)$ and η, is simply achieved by using the stress–strain response of the 0° and 90° tensile and compressive tests and the two functions f_1 and f_2 previously determined. As displayed in Fig. 9, a linear relationship connects the relative change of the compressive compliance to the applied stress, in the initial range where damage does not take place (i.e., $0 > \sigma_i > \sigma_i^{\mathrm{r}}$). The slopes of the straight lines thus obtained then directly provide the values of the constants γ_i governing the non-linear elastic behavior:

$$\begin{aligned} \gamma_1 &= 3.2 \times 10^{-3}\ \mathrm{MPa}^{-1}, \\ \gamma_2 &= 4.4 \times 10^{-3}\ \mathrm{MPa}^{-1}. \end{aligned} \tag{31}$$

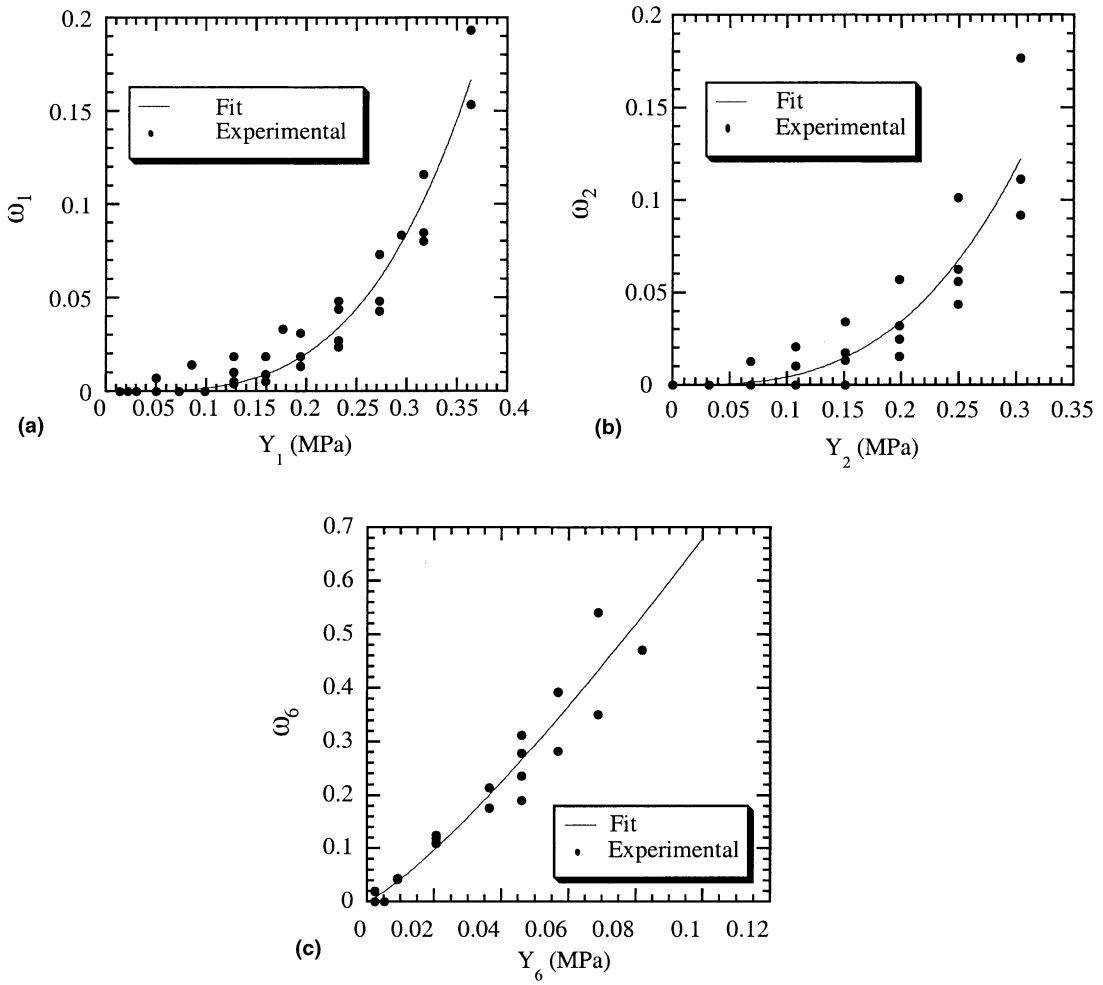

Fig. 8. Experimental and fitted identification of the damage threshold functions f_1 (a), f_2 (b) and f_6 (c).

Following a procedure established in the case of a C/SiC composite (Camus et al., 1996), values of the coefficients of the tensor $\boldsymbol{\sigma}^{r}$, which accounts for the damage-induced partial relaxation of the thermal stresses, are obtained at the concurrent points which grossly connect the compliance slopes derived from the last loading/unloading cycles of the 0° and 90° tensile stress–stain curves. The value of the rate of damage deactivated in compression, coefficient η, is finally obtained by fitting the two damage curves derived from the tests performed in tension and in compression at 0° within the fiber axis. Values of these three coefficients have been established as:

$$\sigma_1^{r} = -40 \text{ MPa}, \quad \sigma_2^{r} = -40 \text{ MPa}, \quad \eta = 0.2. \tag{32}$$

These four aforementioned tests with addition of the 45° off-axis tension test give easily access to the constants defining the rupture criterion, identified as:

$$\tilde{\sigma}_1^{f} = 142 \text{ MPa}, \quad \tilde{\sigma}_2^{f} = 90 \text{ MPa}, \quad \omega_6^{f} = 0.8, \quad W_c^{f} = 230 \text{ kJ/m}^3. \tag{33}$$

The initial assumption of preserved orthotropy all along the loading path allows to consider off-axis tests as being representative of multiaxial propor-

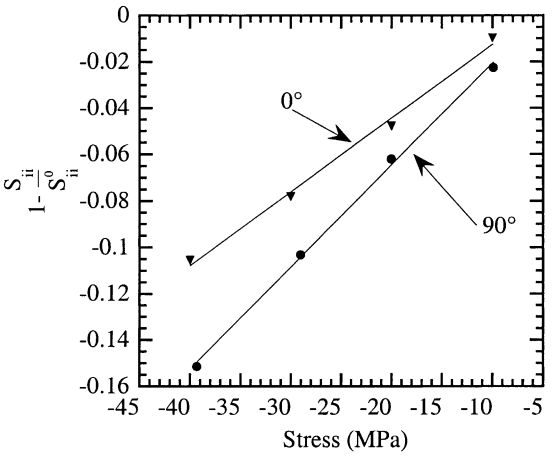

Fig. 9. Relative variation of the compliance as a function of the applied stress for tests performed in compression within the fiber axes.

tional loadings. The identification of the coupling functions g_{ij} may thus be simply achieved by using the three functions f_1, f_2 and f_6 previously determined and the stress–strain responses of 22.5°, 45° and 75° off-axis tensile tests. A simple numerical optimization method is used to calculate the graphs of the two functions g_{ij} appearing in the equation of each damage surface (Eqs. (18a) and (18b), and (19a) and (19b)), by a classical minimization of the difference between the experimental and calculated damage rate. Examples of graphs of some of the coupling functions thus obtained are given in Fig. 10. An appropriate form of evolution laws fitting these functions has been established as:

$$g_{ij}(Y_j) = \frac{m_{ij}}{n_{ij} + Y_j},$$
$$i, j = 1, 2, 6, \quad i \neq j, \text{ no summation}, \tag{34}$$

where coefficients m_{ij} and n_{ij} are normalizing forces.

The final step consists in determining the values of the hardening function and of the constants entering the equation of the threshold surface σ_{eq} which both govern the inelastic residual strains. The strain hardening function $p \to R(p) + R_0$ and constant c are directly obtained from the stress–residual strain response of the tests performed in tension and in compression at 0° from direction 1, using Eq. (20), and the yield condition $h = 0$ (Fig. 11). An appropriate form of evolution law fitting the data shown in Fig. 11 has been established as:

$$R(p) = \alpha p^{\beta} \tag{35}$$

with

$$R_0 = 0, \quad \alpha = 634 \text{ MPa}, \quad \beta = 0.55.$$

Constants a, b, d are then simply determined with the help of tests performed at 90° in tension and in compression, and at 45° in off-axis tension, by collapsing each stress–residual strain response on

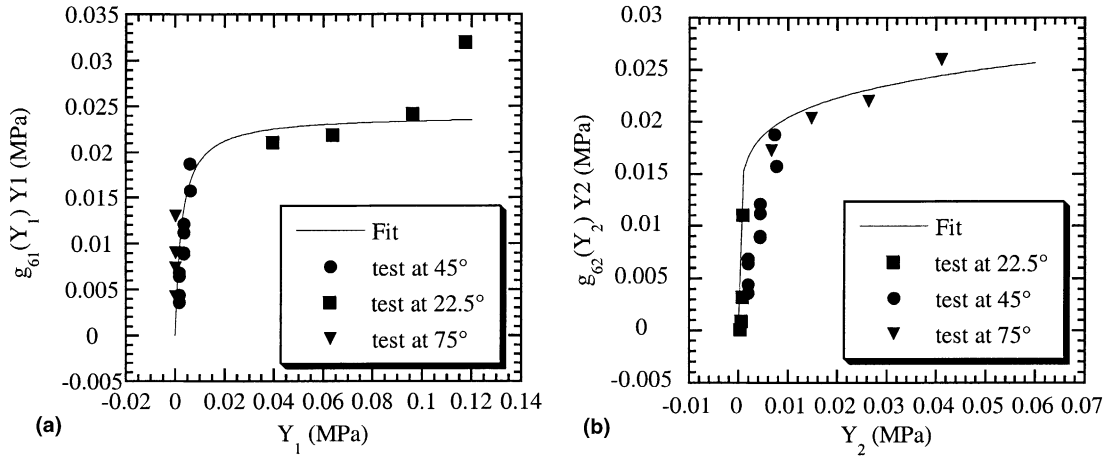

Fig. 10. Experimental and fitted identification of the coupling functions $g_{61}(Y_1)Y_1$ (a) and $g_{62}(Y_2)Y_2$ (b).

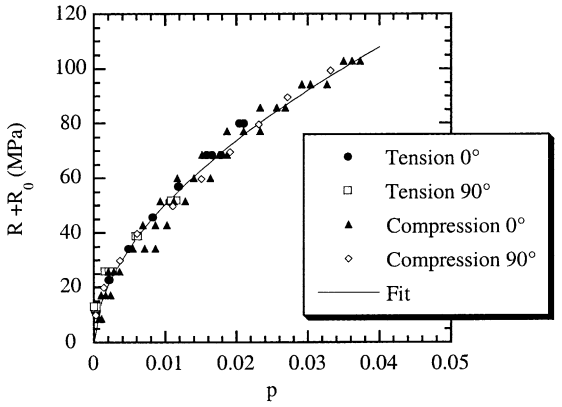

Fig. 11. Experimental and fitted identification of the residual strain hardening function $R(p)$.

the strain hardening curve (Fig. 11). The values retained for these four constants are:

$$a = 1.14, \quad b = 3.24, \quad c = 0.14, \quad d = 0.15. \tag{36}$$

4.2. Experimental verification and discussion

Once the identification procedure has been completed, the constitutive law was then computed in view of performing numerical simulations of the mechanical response of the composite subjected to various loading conditions. It is noted that the explicit character of the elastic-damageable part of the model renders the computational flow chart very simple since no iterative algorithm is locally required at each loading step. Computation of the inelastic residual strains was performed by a classical numerical integration method.

Figs. 12–14 display a comparison between the experiments and the computations of various on-axis and off-axis tension and compression tests. If some of these tests have been used in the identification procedure, tests performed off-axis, at 15° and 67.5° in tension, and at 67.5° in compression represent case tests allowing to measure the ability of the constitutive law to predict the mechanical behavior of the material subjected to different stress states. The fairly good agreement observed between the model and the experiments in terms of stress–strain curves as well as of residual strains and modulus decrease (as derived from interposed unloading/reloading cycles) corroborates the pertinence of the basic assumptions made to build up the model. Likewise, experimental and predicted ultimate failures compare favorably, which also tends to support the validity of the failure criterion. It appears, however, that rupture in tension

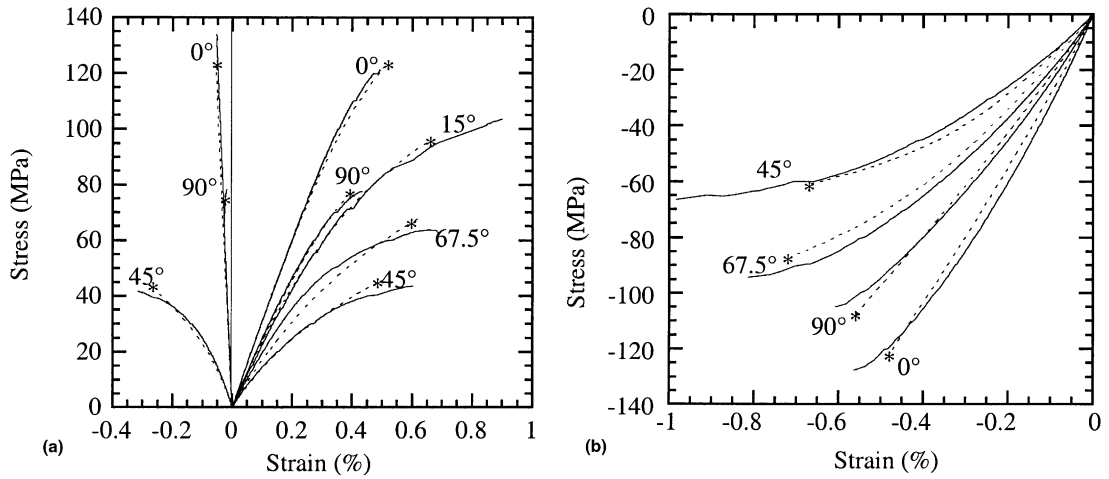

Fig. 12. Comparisons between simulations (dotted lines) and experimental data (solid lines) for tension tests (a) and compression tests (b) performed at various loading angles from direction 1. Stars indicate the calculated failures.

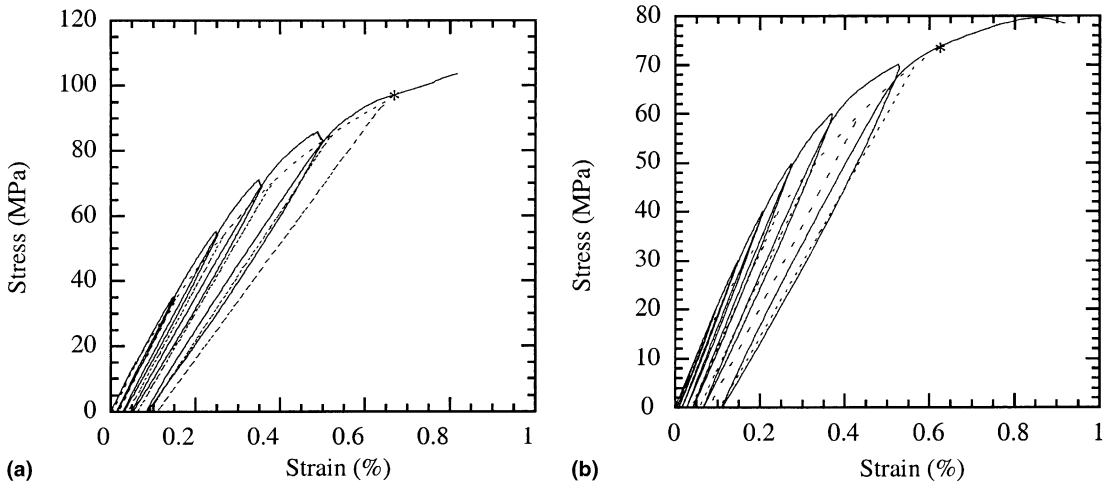

Fig. 13. Comparisons between simulations (dotted lines) and experimental data (solid lines) for cycled tension tests performed at 15° (a) and 67.5° (b) from direction 1.

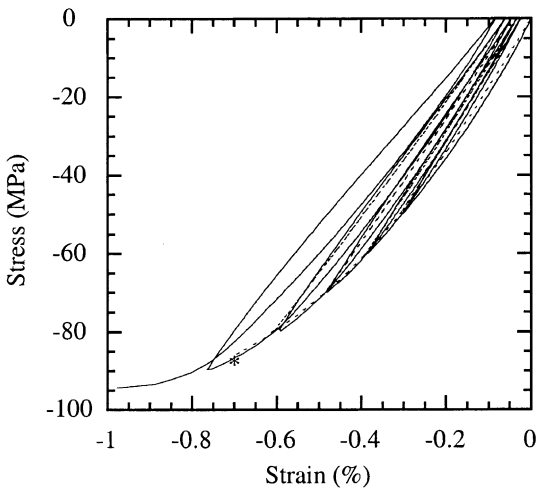

Fig. 14. Comparisons between simulations (dotted lines) and experimental date (solid lines) for a cycled compression test performed at 67.5° from direction 1.

at 67.5° is slightly overestimated whereas, conversely, rupture values of tests performed off-axis in compression tend to be underestimated. In this respect, a more precise comparison between the experimental results and the numerical simulations would certainly require more experiments (i.e. 3/4 tests for each type of loading) in order to define an average behavior of the material including mean rupture values.

Fig. 15 shows a comparison between the experimental and the simulated stress–strain behavior of the material subjected to cyclic tension/compression tests. By contrast with the previous results, a noticeable discrepancy is found if considering damage evolution (i.e. the apparent modulus decrease) for which the model predicts lower values than the experimental ones. Conversely, the inelastic residual strains appear to be in a much closer agreement. Nevertheless, it should be emphasized that the present approach allows to qualitatively retrace the experimental behavior while avoiding to introduce fundamental inadequacy (e.g. strain discontinuity), which was the primary objective regarding this kind of loading. As a matter of fact the observed discrepancy was logically expected, for frictional sliding related effects, which have been neglected in the establishment of the model, seem to play a leading part in the overall non-linear mechanical behavior of the material under cyclic loadings. Additionally, it is very likely that the description of the coupling effects between tensile and compressive damage, deliberetely introduced under the simplest possible form (Eq. (19b)), proves to be somewhat inadequate.

A more accurate description of these two phenomena thus appears to be essential to the modelling of cyclic tension/compression tests.

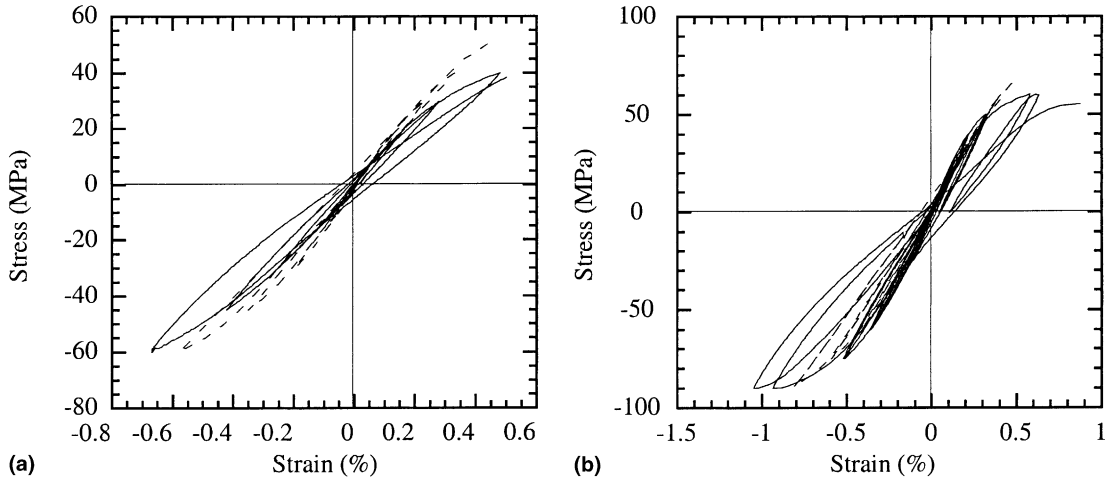

Fig. 15. Comparisons between simulations (dotted lines) and experimental data (solid lines) for cyclic tension/compression tests performed off-axis at 45° (a) and 67.5° (b) from direction 1.

5. Conclusion

A macroscopic model for the non-linear analysis of a 3D C/C composite under complex multiaxial loading has been presented within the framework of continuum damage mechanics. The knowledge of the dominating physical phenomena has helped to condense the model to a minimum complexity, while preserving physical and thermodynamical coherency. The complicated process of damage development and related effects is reduced to the use of four internal scalar variables, three phenomenological damage variables accounting for matrix microcracking and fibre/matrix debonding, and the accumulated plastic strain aimed at modelling the "inelastic" residual strains. The kinetic laws of growth of the damage variables are given by coupled multiple criteria written in the generalized space of associated thermodynamic forces, whereas the occurrence of residual strains is described using a formalism derived from the general plasticity theory. The specific behavior observed in compression, combining non-linear elasticity and partial damage deactivation, has been taken into account through the definition of an effective compliance tensor increment. The set of material dependent functions and parameters intervening in the model may be easily identified from few simple uniaxial tests.

Comparison between experiments and numerical simulations reveal a good ability of the modeling approach for describing the non-linear behavior observed under various on-axis and off-axis uniaxial loading conditions. An important issue yet remaining to be addressed is the incorporation of the hysteretic effects linked to frictional sliding which seem to be no longer negligible under certain loading states such as those encountered in the case of cyclic tension/compression tests. Since all the mechanical tests performed in this work are only representative of multiaxial proportional loading conditions, a more complete verification of the ability of the model will require the use of truly multiaxial tests.

This model is well suited for an easy implementation in standard finite element codes and may thus be used to predict the damage state of a structure during the subcritical stage, i.e. before damage localization.

Acknowledgements

This work has been supported by Snecma-Moteurs and CNRS through a grant to J.P. The authors are indebted to B. Humez for his assistance in the mechanical tests.

References

Allix, O., Ladevèze, P., Vittecoq, F., 1994. Modelling and identification of the mechanical behavior of composite laminates in compression. Comp. Sci. Technol. 51, 35–42.

Baste, S., Audoin, B., 1991. On internal variables in anisotropic damage. Eur. J. Mech. A 10 (6), 587–606.

Bataille, J., Kestin, J., 1979. Irreversible processes and physical interpretations of rational thermodynamics. J. Non-Equil. Thermodyn. 4, 229–258.

Camus, G., Guillaumat, L., Baste, S., 1996. Development of damage in a 2D woven C/SiC composite under mechanical loading: I. mechanical characterization. Comp. Sci. Technol. 56, 1363–1372.

Camus, G., 2000. Modelling of the mechanical behavior and damage processes of fibrous ceramic matrix composites: Application to a 2D SiC/SiC. Int J. Solids Struct. 37 (6), 919–942.

Chaboche, J.L., Lesne, P.M., Maire, J.F., 1995. Macroscopic modelling and damage processes in CMCs. Ceram. Trans. 57, 65–75.

Cluzel, C., Allix, O., Ladevèze, P., Peres, P., 1992. Damage meso-modelling of 3D evolutive composite. In: Bunsell, A.R., Jamet, J.F., Massiah, A. (Eds.), Developments in the Science and Technology of Composite Materials, ECCM5. European Association for Composite Materials, Bordeaux, pp. 591–596.

Dumont, J.P., Ladevèze, P., Poss, M., Remond, Y., 1987. Damage mechanics for 3D composites. Comp. Struct 8, 119–141.

Fung, Y.C., 1965. Foundations of Solid Mechanics. Prentice-Hall, Englewood Cliffs, NJ.

Genin, G.M., Hutchinson, J.W., 1997. Composite laminates in plane stress: constitutive modeling and stress redistribution due to matrix cracking. J. Am. Ceram. Soc. 80 (5), 1245–1255.

Germain, P., Nguyen, Q.S., Suquet, P., 1983. Continuum thermodynamics. J. Appl. Mech. 50, 1010–1020.

Harris, C.E., Lee, J.W., Allen, D.H., 1989. Internal state variable approach for predicting stiffness reduction in fibrous laminated composites with matrix cracks. J. Comp. Mater. 23, 1273–1291.

Kachanov, L.M., 1958. Time of the rupture process under creep conditions. Izv. Akad. Nauk. S.R.S., Odt Tekh. Nauk. 8, 26–31.

Krajcinovic, D., 1989. Damage mechanics. Mech. Mater. 8, 117–197.

Ladevèze, P., 1994. Inelastic strains and damage. In: Talreja, R. (Ed.), Damage Mechanics of Composite Materials. Elsevier, Amsterdam, pp. 117–138.

Ladevèze, P., Gasser, A., Allix, O., 1994. Damage mechanisms modeling for ceramic composites. J. Eng. Mater. Tech. 116, 331–336.

Lemaître, J., Chaboche, J.L., 1985. Mechanics of Solid Materials. Bordas, Paris (in French).

Lemaître, J., 1992. A Course on Damage Mechanics. Springer, Berlin, Heidelberg.

Lubliner, J., 1990. Plasticity Theory. Macmillan, New-York.

Matzenmiller, A., Lubliner, J., Taylor, R.L., 1995. A constitutive model for anisotropic damage in fiber-composites. Mech. Mater. 20, 125–152.

Nguyen, B.N., Laschet, G., Peres, P., 1993. Comparison between numerical strength predictions and experimental results from the tests on tridimensional evolutive Carbon/Carbon specimens under axial loading. In: Naslain, R., Lamon, J., Doumeingts, D. (Eds.), High Temperature Ceramic Matrix Composites, HTCMC1. Woodhead Publishing limited, Abington Hall, pp. 573–581.

Ortiz, M., 1985. A constitutive theory for the inelastic behavior of concrete. Mech. Mater. 4, 67–93.

Savage, G., 1993. Carbon–Carbon Composites. Chapman and Hall, London.

Siron, O., 1996. Approche micro–macro du comportement mécanique et de la rupture d'un composite carbone/carbone à architecture fibreuse multidirectionnelle. Ph.D. thesis, University of Bordeaux, France.

Siron, O., Lamon, J., 1998. Damage and failure mechanisms of a 3-directional carbon/carbon composite under uniaxial tensile and shear loads. Acta Mater. 46 (18), 6631–6643.

Siron, O., Pailhes, J., Lamon, J., 1999. Modelling of the stress/strain behaviour of a carbon/carbon composite with a 2.5 dimensional fibre architecture under tensile and shear loads at room temperature. Comp. Sci. Technol. 59, 1–12.

Talreja, R., 1991. Continuum modelling of damage in ceramic matrix composites. Mech. Mater. 12, 165–180.